

# Deep Reinforcement Learning for Feedback Control in a Collective Flashing Ratchet

Dong-Kyum Kim<sup>1</sup> and Hawoong Jeong<sup>1,2,\*</sup>

<sup>1</sup>Department of Physics, Korea Advanced Institute of Science and Technology, Daejeon 34141, Korea

<sup>2</sup>Center for Complex Systems, Korea Advanced Institute of Science and Technology, Daejeon 34141, Korea

A collective flashing ratchet transports Brownian particles using a spatially periodic, asymmetric, and time-dependent on-off switchable potential. The net current of the particles in this system can be substantially increased by feedback control based on the particle positions. Several feedback policies for maximizing the current have been proposed, but optimal policies have not been found for a moderate number of particles. Here, we use deep reinforcement learning (RL) to find optimal policies, with results showing that policies built with a suitable neural network architecture outperform the previous policies. Moreover, even in a time-delayed feedback situation where the on-off switching of the potential is delayed, we demonstrate that the policies provided by deep RL provide higher currents than the previous strategies.

*Introduction* — A flashing ratchet is a nonequilibrium model that induces a net current of Brownian particles in a spatially periodic asymmetric potential that can be temporally switched on and off [1–4]. If one can access the position information of the particles, the current can be greatly improved by feedback control that switches the potential on-off based on the position information [5]. Feedback strategies for maximizing the current in flashing ratchets have been extensively studied [4–13] due to the model’s applicability in various disciplines [14]; for instance, flashing ratchets have been used for explaining transport phenomena in biological processes such as ion pumping [15], molecular transportation [16], and by motor proteins [17–20]. However, the proposed feedback strategies [4–11] are not optimal policies for a moderate number of particles and require prior information of the system as well.

Thanks to the recent advances in deep learning [21], physicists in diverse fields have been applying it to complex problems that are analytically intractable, e.g. glassy systems [22], quantum matter [23], and others [24]. In particular, reinforcement learning (RL) [25] has shown unprecedented success in previously unsolvable problems through combination with deep neural networks [26–29]. This framework, so-called deep RL, has become a highly efficient tool for quantum feedback control, showing similar or better performance than previous handcrafted policies [30–34]. In this Letter, we employ deep RL to obtain optimal policies in the collective flashing ratchet model, and validate our approach by application to a time-delayed feedback situation that occurs in actual experiments [12].

*Collective flashing ratchet* — We consider the collective flashing ratchet model [5], which consists of an ensemble of  $N$  non-interacting Brownian particles in contact with a heat bath at temperature  $T$  and that drift in a spatially periodic asymmetric potential  $U$ . The dynamics of the  $N$  particles is governed by the following

overdamped Langevin equation:

$$\begin{aligned} \eta \dot{x}_i(t) &= \alpha(s_t)F(x_i(t)) + \xi_i(t); \\ s_t &\equiv \{x_1(t), \dots, x_N(t)\}, \quad i = 1, \dots, N, \end{aligned} \quad (1)$$

where  $x_i(t)$  is the position of particle  $i$ ,  $\eta$  is the friction coefficient, and  $\xi_i$  is a Gaussian noise with zero mean and correlation  $\mathbb{E}[\xi_i(t)\xi_j(t')] = 2\eta k_B T \delta_{ij} \delta(t-t')$  where  $\mathbb{E}$  denotes the ensemble average. Here,  $\alpha$  is a deterministic control policy that depends on a set of positions  $s_t$  with an output of 0 (off) or 1 (on). The force is given by  $F(x) = -\partial_x U(x)$  with the potential [see Fig. 1(a)]

$$U(x) = U_0 \left[ \sin\left(\frac{2\pi x}{L}\right) + \frac{1}{4} \sin\left(\frac{4\pi x}{L}\right) \right]. \quad (2)$$

In all simulations, we set  $L = 1$ ,  $k_B T = 1$ , diffusion coefficient  $D = k_B T / \eta = 1$ ,  $U_0 = 5k_B T$ , and time step size  $\Delta t = 10^{-3} L^2 / D$ . The current of the particles in steady state under policy  $\alpha$  is denoted as

$$\mathbb{E}_\alpha[\dot{x}] \equiv \mathbb{E}_\alpha \left[ \frac{1}{N} \sum_{i=1}^N \dot{x}_i \right] \quad (\text{Unit : } D/L). \quad (3)$$

Various policies for maximizing the current (3) have been proposed as follows: the periodic switching pol-

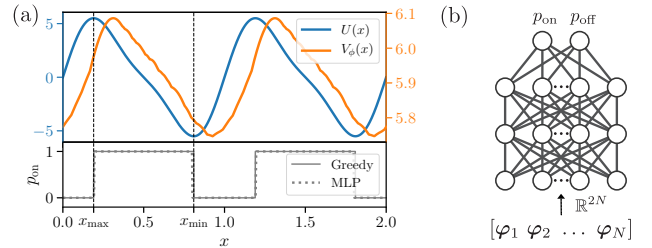


FIG. 1. (a)  $N = 1$  case. Top: Potential  $U$  and trained value network  $V_\phi$  as a function of position  $x$  are denoted by blue and orange lines, respectively. Bottom: The solid line denotes the probability of switching on the potential ( $p_{\text{on}}$ ) as a function of  $x$  for the greedy policy. The dotted line represents  $p_{\text{on}}$  of the trained MLP policy. (b) Illustration of a MLP with two hidden layers for the policy network  $\pi_\theta$ .

icy [4], maximizing instantaneous current (greedy policy) [5], threshold policy [6–8], and Bellman’s criterion [13].

The periodic switching policy [4] is  $\alpha(t) = 1$  for  $t \in [0, \mathcal{T}_{\text{on}})$ ,  $\alpha(t) = 0$  for  $t \in [\mathcal{T}_{\text{on}}, \mathcal{T}_{\text{on}} + \mathcal{T}_{\text{off}})$ , and periodic  $\alpha(t + \mathcal{T}_{\text{on}} + \mathcal{T}_{\text{off}}) = \alpha(t)$  with optimal periods  $\mathcal{T}_{\text{on}} \approx 0.03L^2/D$  and  $\mathcal{T}_{\text{off}} \approx 0.04L^2/D$ . For any  $N$ , this policy gives the current  $\mathbb{E}_\alpha[\dot{x}] \approx 0.862D/L$  because it does not depend on the position but only time.

The greedy policy [5] is defined as  $\alpha(s_t) = \Theta(f(s_t))$ , where  $f(s_t) = \sum_{i=1}^N F(x_i(t))/N$  is the mean force and  $\Theta$  is the Heaviside function given by  $\Theta(z) = 1$  if  $z > 0$  or else 0. While the greedy policy is the optimal one for  $N = 1$ , this policy is outperformed by the periodic switching policy for large  $N$ .

The threshold policy [6–8] is  $\alpha(s_t) = 0$  if  $f(s_t) \leq u_{\text{on}}$  when  $f(t)$  is decreasing, and  $\alpha(s_t) = 1$  if  $f(s_t) \geq u_{\text{off}}$  when  $f(t)$  is increasing, with thresholds  $u_{\text{on}} \geq 0$  and  $u_{\text{off}} \leq 0$ . The threshold policy with optimal thresholds gives mostly similar performance to the greedy policy for  $N < 10^2$ – $10^3$  and is better than the greedy policy for larger  $N$ . It is also optimal for  $N = \infty$ , which is equivalent to the periodic switching policy.

Neither greedy nor threshold policy is optimal for finite  $N > 1$ . Roca *et al.* [13] proposed a general framework for finding the optimal policy via Bellman’s principle, and found it for  $N = 2$  using numerical integration. However, this numerical method requires prior information of the model and is computationally infeasible for large  $N$  due to the curse of dimensionality.

*Methods* — We employ the actor-critic algorithm, which is one of the policy gradient methods in RL [25], together with deep neural networks to find the optimal policies in the collective flashing ratchet for any  $N$ .

To formulate this problem in RL language, we define the reward as the total mean displacement of the particles:

$$r_t = \frac{1}{N} \sum_{i=1}^N (x_i(t + \Delta t) - x_i(t)). \quad (4)$$

The total discounted reward from time  $t$ , called return, is  $G_t = \sum_{k=0}^{\infty} \gamma^k r_{t+(k+1)\Delta t}$  where  $\gamma \in [0, 1)$  is the discounting factor and we set  $\gamma = 0.999$ . We build a policy network  $\pi_\theta$ , called actor, where  $\theta$  denotes the trainable neural network parameters, that takes system state  $s$  as an input. The outputs  $\pi_\theta(s) = (p_{\text{on}}, p_{\text{off}})$  are the probabilities for switching the potential on or off [see Fig. 1(b)]. We sample the on-off probability from  $\pi_\theta(s_t)$  every  $t$  in the training process.

The goal in RL is obtaining the optimal policy  $\pi^*$  that maximizes the expected total future reward, i.e.  $\pi^* = \arg \max_\pi \mathbb{E}_\pi[G_t]$ . If the equation of motion is known,  $\mathbb{E}_\pi[G_t]$  can be numerically calculated using Bellman’s equation [13]. However, in this work, we assume that we can only access the system state  $s_t$  and reward  $r_t$ .

In such case, called model-free RL, we need an estimator  $V_\phi$  for a *value function*:

$$V^\pi(s_t) = \mathbb{E}_\pi[G_t | s_t], \quad (5)$$

which is the expected return given state  $s_t$  under a policy  $\pi$ . The estimator  $V_\phi$ , called value network or critic, where  $\phi$  denotes the trainable parameters, is also built with another neural network.

There are various optimization methods for the actor-critic algorithm [35]. Among them, we employ proximal policy optimization [36], which is widely used in RL because of its scalability, data efficiency, and robustness for hyperparameters (see Supplemental Material [37] for training details). After the training process is complete, we test the policy deterministically, i.e.

$$\alpha(s_t) = \begin{cases} 1 & \text{if } p_{\text{on}} > 0.5 \\ 0 & \text{if } p_{\text{off}} > 0.5, \end{cases} \quad \text{where } (p_{\text{on}}, p_{\text{off}}) = \pi_\theta(s_t).$$

*Neural network architecture* — First, we employ multilayer perceptron (MLP) architecture for the policy network  $\pi_\theta$  and value network  $V_\phi$  [see Fig. 1(b)]. The configuration details of the neural network architectures are given in the Supplemental Material [37]. Using the periodicity of the potential  $U(x)$ , we transform the state  $s_t$  into the input feature  $\psi_t = [\varphi_1(t), \varphi_2(t), \dots, \varphi_N(t)]$  for neural network input where

$$\varphi_i(t) = \left[ \cos\left(\frac{2\pi x_i(t)}{L}\right), \sin\left(\frac{2\pi x_i(t)}{L}\right) \right]. \quad (6)$$

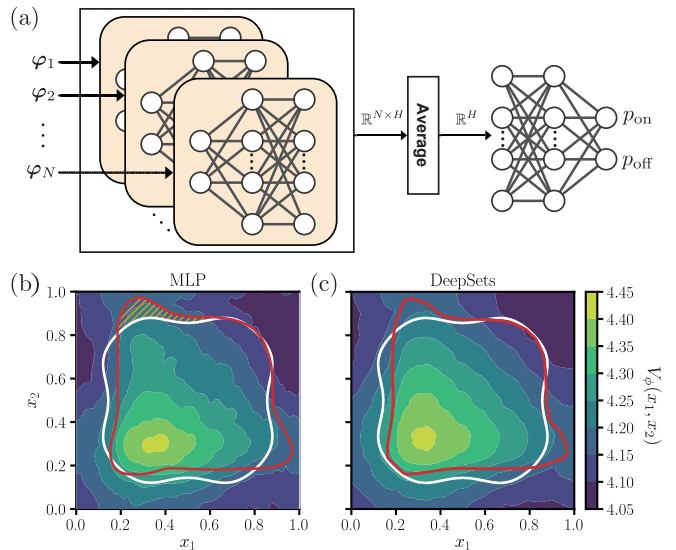


FIG. 2. (a) DeepSets architecture for the policy network  $\pi_\theta$ .  $H$  is the number of hidden units for each layer. (b,c) Decision boundaries from a trained MLP (b) and trained DeepSets (c) for  $N = 2$ . The white contour denotes where the mean force  $f(x_1, x_2)$  is zero. The red contour is  $p_{\text{on}} = 0.5$  from the trained policy network  $\pi_\theta$ . The color gradient represents the trained value network  $V_\phi$ .

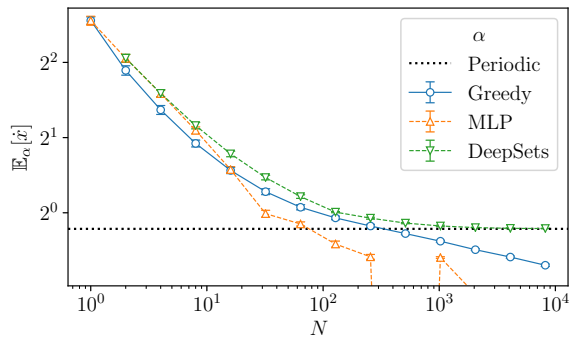


FIG. 3. Current  $\mathbb{E}_\alpha[x]$  as function of  $N$  for each policy  $\alpha$ . Throughout this work, error bars represent the standard deviation of the current measured from the realized trajectory ensemble over the period  $t = 50L^2/D$ .

Therefore, the number of input nodes of the MLP is  $2N$  and the number of output nodes is two for  $\pi_\theta$ . The value network  $V_\phi$  has the same architecture, except that it has a single output node rather than two output nodes. We note that the discounting factor  $\gamma = 0.999$ , which indicates the return  $G_t$ , can effectively be considered as the total mean displacement between  $t$  and  $t + \Delta t/(1 - \gamma)$ . Accordingly,  $V_\phi(\psi_t)$  can be interpreted as the expected current given  $\psi_t$  because the time step size is  $\Delta t = 10^{-3}L^2/D$ .

For the  $N = 1$  case, Fig. 1(a) shows that the trained  $\pi_\theta$  agrees with the greedy policy (bottom panel), while  $V_\phi$  is slightly shifted to the right from potential  $U$  (top panel). This is because, at the top of the potential valley ( $x_{\max}$ ), the particle can slide to the right or left with a 50/50 chance, and therefore the expected current is maximum slightly right of  $x_{\max}$ .

For the  $N = 2$  case, as shown in Fig. 2(b), the greedy policy switches on (off) the potential when the particles are inside (outside) the white contour. On the other hand, the decision boundary of the trained MLP policy  $\pi_\theta$  (red contour) agrees with the policy discovered by Roca *et al.* [13] and shows better performance than the greedy policy by considering the future expected current. For instance, in the orange dashed area, the instantaneous net current will be negative because the mean force  $f(x_1, x_2)$  is negative when the potential is on. But considering each particle with a long-term view, particle 1 and particle 2 are located on the downhill of the potential ( $x_{\max} < x < x_{\min}$ ) and near the minimum ( $x_{\min}$ ), respectively; while particle 2 will soon reach  $x_{\min}$  and become trapped in the potential well, particle 1 can keep moving down along the potential [13].

However, the decision boundary (red contour) and  $V_\phi$  (color gradient) are not symmetric over the line  $x_1 = x_2$  [see Fig. 2(b)] because MLP outputs are not permutation invariant to the order of the elements in the input feature  $\psi_t$ . To address this issue, we employ a permutation invariant architecture, called DeepSets [38], for the policy

and value networks. In this architecture [see Fig. 2(a)], each element  $\varphi_i$  in the input feature  $\psi_t$  is independently fed into a single MLP (beige), and the outputs of the MLP are averaged over the elements and then fed into another MLP. By using DeepSets for training, the decision boundary and  $V_\phi$  show perfect symmetry over the  $x_1 = x_2$  line [see Fig. 2(c)].

Now we apply these methods for  $N = 2^2, 2^3, \dots, 2^{13}$ , and compare the training results with the greedy (blue circles) and periodic switching (black dotted line) policies in Fig. 3. Results show that the trained MLP policies (orange triangles) outperform the greedy policy for  $N < 10$ , but perform poorly for  $N > 10$  due to the lack of permutation invariance. On the other hand, the trained DeepSets policies (green triangles) outperform the other policies for any  $N > 1$  while converging to the periodic policy as  $N$  increases (see Fig. S1, Supplemental Material [37]). We have also verified that deep RL works well for the sawtooth potential (Fig. S2, Supplemental Material [37]).

*Time-delayed feedback* — In an actual experiment, there is an inevitable time-delay between the measurement and the feedback due to the calculation time in the feedback algorithm [9–12]. To verify that deep RL is applicable to such a realistic situation, we consider a feedback time-delay  $\tau$  in Eq. (1), i.e.  $\alpha(s_t)$  is replaced by  $\alpha(s_{t-\tau})$ . In this case, the maximal net displacement

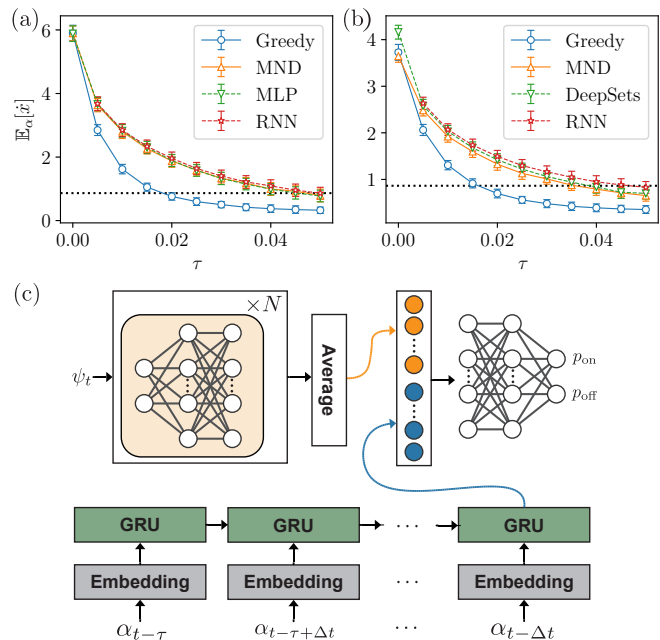


FIG. 4. Time-delayed feedback results for (a)  $N = 1$  and (b)  $N = 2$ . The black dotted lines denote the current of the periodic switching policy. (c) Architecture of policy network  $\pi_\theta$  augmented with a RNN.

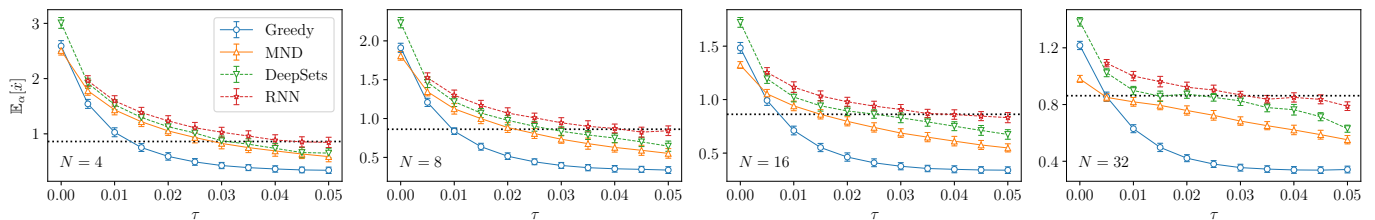


FIG. 5. Time-delayed feedback results for the greedy, MND, DeepSets, and RNN policies at increasing  $N$  from left to right. The black dotted lines denote the current from the periodic switching policy.

(MND) policy [11], defined by

$$\alpha(s_{t-\tau}) = \Theta \left( \sum_{i=1}^N d(x_i(t-\tau)) \right), \quad (7)$$

where the displacement function is  $d(x) = x_{\min} + x_0 - x$  for  $x_{\max} < x \leq x_{\max} + L$  and periodic  $d(x) = d(x + L)$ , can perform better than the greedy policy for  $\tau > 0$  with optimal  $x_0 < 0$  [12]. This can be considered as a  $\tau$ -delayed greedy policy because it predicts the arrival of the particles at  $x_{\min}$  after  $\tau$  from  $x_0 + x_{\min}$ . We train the neural networks for  $N = 1, 2^1, 2^2, \dots, 2^5$  with time-delay  $\tau$  in the range of 0.00–0.05 $L^2/D$ , and compare them with the greedy policy and the MND policy with optimal  $x_0$ .

For the time-delayed  $N = 1$  case [see Fig. 4(a)], the results show that the trained MLP policies (green triangles) agree with the MND policy (orange triangles) and perform better than the greedy policy (blue circles). For  $N = 2$ , the trained DeepSets policies (green triangles) outperform the greedy policy and are slightly better than the MND policy [see Fig. 4(b)].

While the actor-critic algorithm assumes that the feedback-controlled system is a Markov decision process (MDP), the delayed-feedback process is not a MDP because the next state  $s_{t+\Delta t}$  not only depends on the previous state  $s_t$  but also the history of the on-off information. This problem can be reformulated as a MDP by augmenting the input feature  $\psi_t$  with the on-off history [39]. Here, the  $d$ -step augmented state at time  $t$  is defined as

$$I_t = (\alpha_{t-\tau}, \alpha_{t-\tau+\Delta t}, \dots, \alpha_{t-\tau+(d-1)\Delta t}, \psi_t), \quad d = \tau/\Delta t.$$

In order to efficiently handle the augmented state, we build the policy network with a recurrent neural network (RNN). We employ an embedding layer to transform the discrete variable  $\alpha$  into a continuous variable and use a gated recurrent unit (GRU) [40] for the RNN. As shown in Fig. 4(c), we concatenate the output vectors from DeepSets (orange nodes) and the RNN (blue nodes), where DeepSets and the RNN encode the position information  $\psi_t$  and potential on-off history, respectively. We then feed the concatenated vector to a MLP. See the Supplemental Material [37] for the configuration details. As can be seen in Fig. 4(a) and 4(b), the trained RNN policies (red stars) show slightly better performance

than the other policies for  $N = 1$  and noticeably better performance than the others for  $N = 2$ . Figure 5 shows that RNN policies also outperform the greedy, MND, and DeepSets policies for the  $N = 4, 8, 16, 32$  cases.

*Conclusions and outlook* — We have tackled the problem of finding an improved policy for maximizing the current in the collective flashing ratchet model through deep RL. Unlike the previous model-based method [13], the model-free RL approach used in this study does not require information on the parameters of the system (e.g. potential, diffusion coefficient, and others). The deep RL approach makes it possible to find state-of-the-art feedback strategies using suitable neural network architectures through training only in the process of interacting with the environment. Also, we have demonstrated that deep RL outperforms the previous strategies in a time-delayed feedback situation; therefore, we expect that this study can be effectively applied experimentally.

Although feedback control in the collective flashing ratchet can induce an effective coupling between non-interacting particles, molecular motors like kinesin, for example, explicitly interact with each other via hardcore repulsion. According to previous studies on interacting molecular motors [17–19], their cooperative behavior can enhance transportation ability several times or more compared to individual motors. Further research applying deep RL on interacting molecular motors will be intriguing.

In real-world scenarios, there may be measurement or feedback errors due to instrument noise [41–43]. Such cases are not only important in physics, e.g. information thermodynamics [44], but also in RL for real-world applications [45]. Therefore, it will also be an interesting future work to study RL from a thermodynamics perspective; we expect that the collective flashing ratchet model can be utilized as a useful environment to benchmark RL algorithms in such situations.

The results of all runs and the code implemented in PyTorch [46] are available in Ref. [47].

This study was supported by the Basic Science Research Program through the National Research Foundation of Korea (NRF) (Grant No. NRF-2017R1A2B3006930).

- 
- \* [hjeong@kaist.edu](mailto:hjeong@kaist.edu)
- [1] J. Prost, J.-F. Chauwin, L. Peliti, and A. Ajdari, Asymmetric pumping of particles, *Phys. Rev. Lett.* **72**, 2652 (1994).
  - [2] R. D. Astumian and M. Bier, Fluctuation driven ratchets: Molecular motors, *Phys. Rev. Lett.* **72**, 1766 (1994).
  - [3] R. D. Astumian, Thermodynamics and Kinetics of a Brownian Motor, *Science* **276**, 917 (1997).
  - [4] M. B. Tarlie and R. D. Astumian, Optimal modulation of a Brownian ratchet and enhanced sensitivity to a weak external force, *Proc. Natl. Acad. Sci. U.S.A.* **95**, 2039 (1998).
  - [5] F. J. Cao, L. Dinis, and J. M. R. Parrondo, Feedback Control in a Collective Flashing Ratchet, *Phys. Rev. Lett.* **93**, 040603 (2004).
  - [6] L. Dinis, J. M. R. Parrondo, and F. J. Cao, Closed-loop control strategy with improved current for a flashing ratchet, *Europhys. Lett.* **71**, 536 (2005).
  - [7] M. Feito and F. J. Cao, Threshold feedback control for a collective flashing ratchet: Threshold dependence, *Phys. Rev. E* **74**, 041109 (2006).
  - [8] M. Feito and F. J. Cao, Optimal operation of feedback flashing ratchets, *J. Stat. Mech.* **2009**, P01031 (2009).
  - [9] M. Feito and F. J. Cao, Time-delayed feedback control of a flashing ratchet, *Phys. Rev. E* **76**, 061113 (2007).
  - [10] E. M. Craig, B. R. Long, J. M. R. Parrondo, and H. Linke, Effect of time delay on feedback control of a flashing ratchet, *Europhys. Lett.* **81**, 10002 (2007).
  - [11] E. M. Craig, N. J. Kuwada, B. J. Lopez, and H. Linke, Feedback control in flashing ratchets, *Ann. Phys.* **17**, 115 (2008).
  - [12] B. J. Lopez, N. J. Kuwada, E. M. Craig, B. R. Long, and H. Linke, Realization of a Feedback Controlled Flashing Ratchet, *Phys. Rev. Lett.* **101**, 220601 (2008).
  - [13] F. Roca, J. P. G. Villaluenga, and L. Dinis, Optimal protocol for a collective flashing ratchet, *Europhys. Lett.* **107**, 10006 (2014).
  - [14] P. Reimann, Brownian motors: noisy transport far from equilibrium, *Physics reports* **361**, 57 (2002).
  - [15] Z. Siwy and A. Fuliński, Fabrication of a Synthetic Nanopore Ion Pump, *Phys. Rev. Lett.* **89**, 198103 (2002).
  - [16] I. Kosztin and K. Schulten, Fluctuation-Driven Molecular Transport Through an Asymmetric Membrane Channel, *Phys. Rev. Lett.* **93**, 238102 (2004).
  - [17] O. Campàs, Y. Kafri, K. B. Zeldovich, J. Casademunt, and J.-F. Joanny, Collective Dynamics of Interacting Molecular Motors, *Phys. Rev. Lett.* **97**, 038101 (2006).
  - [18] J. Brugués and J. Casademunt, Self-Organization and Cooperativity of Weakly Coupled Molecular Motors under Unequal Loading, *Phys. Rev. Lett.* **102**, 118104 (2009).
  - [19] D. Oriola and J. Casademunt, Cooperative Force Generation of KIF1A Brownian Motors, *Phys. Rev. Lett.* **111**, 048103 (2013).
  - [20] W. Hwang and M. Karplus, Structural basis for power stroke vs. Brownian ratchet mechanisms of motor proteins, *Proc. Natl. Acad. Sci. U.S.A.* **116**, 19777 (2019).
  - [21] I. Goodfellow, Y. Bengio, and A. Courville, *Deep Learning* (MIT Press, Cambridge, MA, 2016).
  - [22] V. Bapst, T. Keck, A. Grabska-Barwińska, C. Donner, E. D. Cubuk, S. S. Schoenholz, A. Obika, A. W. R. Nelson, T. Back, D. Hassabis, and P. Kohli, Unveiling the predictive power of static structure in glassy systems, *Nat. Phys.* **16**, 448 (2020).
  - [23] J. Carrasquilla, Machine learning for quantum matter, *Advances in Physics: X* **5**, 1797528 (2020).
  - [24] G. Carleo, I. Cirac, K. Cranmer, L. Daudet, M. Schuld, N. Tishby, L. Vogt-Maranto, and L. Zdeborová, Machine learning and the physical sciences, *Rev. Mod. Phys.* **91**, 045002 (2019).
  - [25] R. S. Sutton and A. G. Barto, *Reinforcement learning: An introduction* (MIT Press, Cambridge, MA, 2018).
  - [26] V. Mnih *et al.*, Human-level control through deep reinforcement learning, *Nature (London)* **518**, 529 (2015).
  - [27] D. Silver *et al.*, Mastering the game of Go with deep neural networks and tree search, *Nature (London)* **529**, 484 (2016).
  - [28] D. Silver, T. Hubert, J. Schrittwieser, I. Antonoglou, M. Lai, A. Guez, M. Lanctot, L. Sifre, D. Kumaran, T. Graepel, T. Lillicrap, K. Simonyan, and D. Hassabis, A general reinforcement learning algorithm that masters chess, shogi, and Go through self-play, *Science* **362**, 1140 (2018).
  - [29] O. Vinyals *et al.*, Grandmaster level in StarCraft II using multi-agent reinforcement learning, *Nature (London)* **575**, 350 (2019).
  - [30] T. Fösel, P. Tighineanu, T. Weiss, and F. Marquardt, Reinforcement Learning with Neural Networks for Quantum Feedback, *Phys. Rev. X* **8**, 031084 (2018).
  - [31] R. Porotti, D. Tamascelli, M. Restelli, and E. Prati, Coherent transport of quantum states by deep reinforcement learning, *Commun. Phys.* **2**, 61 (2019).
  - [32] M. Y. Niu, S. Boixo, V. N. Smelyanskiy, and H. Neven, Universal quantum control through deep reinforcement learning, *npj Quantum Inf.* **5**, 33 (2019).
  - [33] Z. An and D. L. Zhou, Deep reinforcement learning for quantum gate control, *Europhys. Lett.* **126**, 60002 (2019).
  - [34] Z. T. Wang, Y. Ashida, and M. Ueda, Deep Reinforcement Learning Control of Quantum Cartpoles, *Phys. Rev. Lett.* **125**, 100401 (2020).
  - [35] J. Achiam, Spinning Up in Deep Reinforcement Learning (2018), <https://spinningup.openai.com>.
  - [36] J. Schulman, F. Wolski, P. Dhariwal, A. Radford, and O. Klimov, Proximal policy optimization algorithms, [arXiv:1707.06347](https://arxiv.org/abs/1707.06347).
  - [37] See Supplemental Material at [SM]. The Supplemental Material includes Refs. [35, 36, 46, 48–50].
  - [38] M. Zaheer, S. Kottur, S. Ravanbakhsh, B. Póczos, R. R. Salakhutdinov, and A. J. Smola, Deep Sets, in *Advances in Neural Information Processing Systems 30* (Curran Associates, Inc., Long Beach, CA, 2017) pp. 3391–3401.
  - [39] K. V. Katsikopoulos and S. E. Engelbrecht, Markov decision processes with delays and asynchronous cost collection, *IEEE Trans. Automat. Contr.* **48**, 568 (2003).
  - [40] K. Cho, B. van Merriënboer, C. Gulcehre, D. Bahdanau, F. Bougares, H. Schwenk, and Y. Bengio, Learning Phrase Representations using RNN Encoder–Decoder for Statistical Machine Translation, in *Proceedings of the 2014 Conference on Empirical Methods in Natural Language Processing (EMNLP)* (Association for Computational Linguistics, Doha, Qatar, 2014) pp. 1724–1734.
  - [41] F. J. Cao, M. Feito, and H. Touchette, Information and flux in a feedback controlled Brownian ratchet, *Physica A* **388**, 113 (2009).

- [42] F. J. Cao and M. Feito, Thermodynamics of feedback controlled systems, *Phys. Rev. E* **79**, 041118 (2009).
- [43] T. Sagawa and M. Ueda, Nonequilibrium thermodynamics of feedback control, *Phys. Rev. E* **85**, 021104 (2012).
- [44] J. M. R. Parrondo, J. M. Horowitz, and T. Sagawa, Thermodynamics of information, *Nat. Phys.* **11**, 131 (2015).
- [45] G. Dulac-Arnold, N. Levine, D. J. Mankowitz, J. Li, C. Paduraru, S. Goyal, and T. Hester, An empirical investigation of the challenges of real-world reinforcement learning, [arXiv:2003.11881](https://arxiv.org/abs/2003.11881).
- [46] A. Paszke *et al.*, PyTorch: An Imperative Style, High-Performance Deep Learning Library, in *Advances in Neural Information Processing Systems 32* (Curran Associates, Inc., Vancouver, 2019) pp. 8024–8035.
- [47] <https://github.com/kdkyum/RatchetDRL>.
- [48] V. Nair and G. E. Hinton, Rectified linear units improve restricted boltzmann machines, in *Proceedings of the 27th International Conference on Machine Learning* (Haifa, Israel, 2010) pp. 807–814.
- [49] D. P. Kingma and J. Ba, Adam: A Method for Stochastic Optimization, in *International Conference on Learning Representations* (2015) [arXiv:1412.6980](https://arxiv.org/abs/1412.6980).
- [50] J. Schulman, P. Moritz, S. Levine, M. Jordan, and P. Abbeel, High-Dimensional Continuous Control Using Generalized Advantage Estimation, in *International Conference on Learning Representations* (2016) [arXiv:1506.02438](https://arxiv.org/abs/1506.02438).

# Supplemental Material: Deep Reinforcement Learning for Feedback Control in a Collective Flashing Ratchet

Dong-Kyum Kim<sup>1</sup> and Hawoong Jeong<sup>1,2,\*</sup>

<sup>1</sup>*Department of Physics, Korea Advanced Institute of Science and Technology, Daejeon 34141, Korea*

<sup>2</sup>*Center for Complex Systems, Korea Advanced Institute of Science and Technology, Daejeon 34141, Korea*

## I. TRAINING DETAILS

We use the proximal policy optimization (PPO) [1] algorithm implemented in Ref. [2]. The PPO algorithm updates the parameter  $\theta_i$  of policy network  $\pi_\theta$  at epoch  $i$  by the following equations:

$$\theta_{i+1} = \arg \max_{\theta} L(\theta), \quad (\text{S1})$$

$$L(\theta) = \mathbb{E}_{(s,a) \sim \pi_{\theta_i}} \left[ \min \left( \frac{\pi_\theta(s,a)}{\pi_{\theta_i}(s,a)} A^{\pi_{\theta_i}}(s,a), g(\epsilon, A^{\pi_{\theta_i}}(s,a)) \right) \right], \quad (\text{S2})$$

where  $\pi_\theta(s,a)$  is the probability of choosing action  $a$  given the state  $s$ , and  $\epsilon$  is a hyperparameter that restricts how much the new policy can be changed from the old policy. Function  $g$  is defined as

$$g(\epsilon, A) = \begin{cases} (1 + \epsilon)A & \text{if } A \geq 0 \\ (1 - \epsilon)A & \text{if } A < 0. \end{cases} \quad (\text{S3})$$

Here,  $A^\pi(s,a)$  is the advantage function that indicates how much better or worse the action  $a$  is than the other actions on average for the present policy  $\pi$  and given state  $s$ . In this section,  $t$  represents the time step, rather than time, for convenience. The definition of  $A^\pi(s_t, a_t)$  is

$$A^\pi(s_t, a_t) = Q^\pi(s_t, a_t) - V^\pi(s_t), \quad (\text{S4})$$

where  $Q^\pi(s_t, a_t) = \mathbb{E}_\pi[G_t | s_t, a_t]$  and  $V^\pi(s_t) = \mathbb{E}_\pi[G_t | s_t]$  are the action-value function and the value function, respectively. The return  $G_t$  is defined as  $G_t = \sum_{l=0}^{\infty} \gamma^l r_{t+l+1}$  where  $\gamma$  is the discounting factor. PPO uses the generalized advantage estimator (GAE) [3]  $\hat{A}_t^{\text{GAE}(\gamma, \lambda)}$  for an accurate evaluation of the advantage function.  $\hat{A}_t^{\text{GAE}(\gamma, \lambda)}$  is defined as

$$\hat{A}_t^{\text{GAE}(\gamma, \lambda)} = \sum_{l=0}^{\infty} (\gamma \lambda)^l \delta_{t+l}^V, \quad (\text{S5})$$

$$\delta_t^V = \underbrace{r_t + \gamma V^\pi(s_{t+1}) - V^\pi(s_t)}_{=Q^\pi(s_t, a_t)}, \quad (\text{S6})$$

where  $\lambda \in (0, 1]$  is a hyperparameter for adjusting the bias-variance tradeoff in  $\hat{A}_t^{\text{GAE}(\gamma, \lambda)}$ . See Algorithm 1 for the detailed training procedure. The policy and value networks are initialized with the default random initialization setup in PyTorch [4]. Two Adam [5] optimizers are used respectively for the policy and value networks training. During the stochastic gradient ascent stage for the policy network (step 4 in Algorithm 1), the early stopping method is applied to prevent the updated policy from going too far from the old policy [2]. Early stopping means that if the Kullback–Leibler divergence (KLD) from the updated policy  $\pi_\theta$  to the old policy  $\pi_{\theta_i}$

$$D_{\text{KL}}(\pi_{\theta_i} \parallel \pi_\theta) = \mathbb{E}_{(s,a) \sim \pi_{\theta_i}} \left[ \log \frac{\pi_{\theta_i}(s,a)}{\pi_\theta(s,a)} \right] \quad (\text{S7})$$

exceeds the threshold  $1.5 \times d_{\text{targ}}$ , then the gradient steps stop. See Table I for the values of all the hyperparameters used in the training. For each  $N$ , we run Algorithm 1 five times independently with five different random seeds, and we pick the policy and value network that show the best performance among the five. All reported results in this paper are from the best-performing neural networks. Each run was conducted on a single NVIDIA TITAN V GPU.

**Algorithm 1** Proximal policy optimization algorithm

**Require:** Environment, policy network  $\pi_\theta$ , value network  $V_\phi$ , optimizer for  $\theta$ , optimizer for  $\phi$

1: **for**  $i = 1, 2, \dots, \mathcal{E}$  **do**

2: Run simulation of multiple trajectories simultaneously under the present policy network  $\pi_{\theta_i}$  in the environment and collect the dataset  $\mathcal{D}_i = \{\Gamma^{(m)}\}_{m=1}^M$  where  $M$  is the number of trajectories. Here,  $\Gamma$  denotes the trajectory of the state, action, and reward, and can be represented as  $\Gamma = [s_1, a_1, r_1, s_2, a_2, r_2, s_3, \dots, r_T, s_{T+1}]$  where  $T$  is the length of a single trajectory.

3: Compute estimated return

$$\hat{G}_t = \sum_{l=0}^{T-t-1} \left( \gamma^l r_{t+l+1} \right) + \gamma^{T-t} V^\pi(s_{T+1}),$$

$\delta_t^V$  (S6), and  $\hat{A}_t^{\text{GAE}(\gamma, \lambda)}$  (S5) for all time step  $t$  and trajectory  $\Gamma$  in  $\mathcal{D}_i$  using the present value network  $V^\pi = V_{\phi_i}$ .

4: Update the policy network by maximizing the estimated  $L(\theta)$  (S2):

$$\theta_{i+1} = \arg \max_{\theta} \frac{1}{MT} \sum_{\Gamma \in \mathcal{D}_i} \sum_{t=1}^T \min \left( \frac{\pi_\theta(s_t, a_t)}{\pi_{\theta_i}(s_t, a_t)} \hat{A}_t^{\text{GAE}(\gamma, \lambda)}, g(\epsilon, \hat{A}_t^{\text{GAE}(\gamma, \lambda)}) \right),$$

via the optimizer for  $\theta$  with a mini-batch size of  $\mathcal{B}$ .

5: Update the value network by minimizing the mean-squared error:

$$\phi_{i+1} = \arg \min_{\phi} \frac{1}{MT} \sum_{\Gamma \in \mathcal{D}_i} \sum_{t=1}^T \left( \hat{G}_t - V_\phi(s_t) \right)^2,$$

via the optimizer for  $\phi$  with a mini-batch size of  $\mathcal{B}$ .

6: **end for**

Hyperparameter	Value						
Trajectory length $T$	2000	$N$	$M$	$\mathcal{B}$	$N$	$M$	$\mathcal{B}$
Number of epochs $\mathcal{E}$	400	1	1024	4096	128	8	256
Discounting factor $\gamma$	0.999	2	512	4096	256	8	256
GAE parameter $\lambda$	0.95	4	256	4096	512	8	256
Clipping parameter $\epsilon$	0.2	8	128	4096	1024	8	256
Target KLD for early stopping $d_{\text{targ}}$	0.01	16	64	2048	2048	8	256
Training iterations for $\pi_\theta$ per epoch	625	32	32	1024	4096	8	256
Training iterations for $V_\phi$ per epoch	625	64	16	512	8192	8	256
Learning rate for $\pi_\theta$	$3 \times 10^{-4}$						
Learning rate for $V_\phi$	$10^{-3}$						

TABLE I. Left: Hyperparameters. The hyperparameters not listed in this table are set as defaults in PyTorch. Right: The number of trajectories  $M$  and mini-batch size  $\mathcal{B}$  for each number of particles  $N$ .

## II. ARCHITECTURE CONFIGURATIONS

We use ReLU [6] as the activation function for the policy network  $\pi_\theta$  and value network  $V_\phi$ . See Tables II, III, and IV for configuration details of the MLP, DeepSets, and RNN policy networks, respectively. The policy network  $\pi_\theta$  computes the on-off probabilities using the softmax function in the output layer. The value network  $V_\phi$  has the same configuration except for having an output dimension of one rather than two. We set the number of hidden units to  $H = 64$  and the embedding dimension to  $E = 16$ . Here,  $\alpha_t^d$  is the potential on-off history:

$$\alpha_t^d = (\alpha_{t-\tau}, \alpha_{t-\tau+\Delta t}, \dots, \alpha_{t-\tau+(d-1)\Delta t}), \quad d = \tau/\Delta t. \quad (\text{S8})$$



MLP policy network		
Layer	Output dim	Activation function
Input $\psi_t$	$2N$	
Fully-connected	$H$	ReLU
Fully-connected	$H$	ReLU
Output layer	2	None

TABLE II. Two-hidden-layer MLP configuration.

DeepSets policy network		
Layer	Output dim	Activation function
Input $\psi_t$	$N \times 2$	
Fully-connected	$N \times H$	ReLU
Fully-connected	$N \times H$	None
Average	$H$	
Fully-connected	$H$	ReLU
Output layer	2	None

TABLE III. DeepSets configuration.

RNN policy network			
Module	Layer	Output dim	Activation function
DeepSets( $\psi_t$ )	Input $\psi_t$	$N \times 2$	
	Fully-connected	$N \times H$	ReLU
	Fully-connected	$N \times H$	None
	Average	$H$	
RNN( $\alpha_t^d$ )	Embedding $\alpha_t^d$	$d \times E$	
	GRU( $\alpha_t^d$ ) last output	$2E$	
MLP	Concatenate [DeepSets( $\psi_t$ ), RNN( $\alpha_t^d$ )]	$H + 2E$	
	Fully-connected	$H$	ReLU
	Output layer	2	None

TABLE IV. RNN configuration.

### III. POLICY AND VALUE NETWORKS OVER TIME

Figure S1 shows that with increasing  $N$ , the deterministic control  $\alpha(t)$  of the trained DeepSets policy as a function of time  $t$  converges with that of the periodic switching policy.

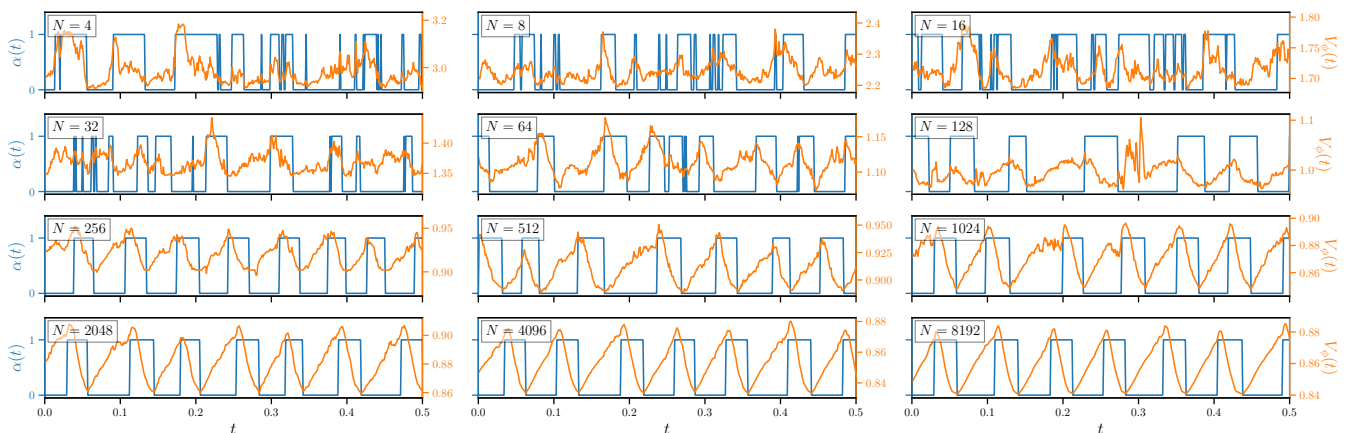


FIG. S1. Policy and value networks over time. The blue and orange lines denote  $\alpha(t)$  and  $V_\phi(t)$ , respectively, as a function of time  $t$  for  $N = 2^2, 2^3, \dots, 2^{13}$ .

#### IV. SAWTOOTH POTENTIAL

We also test the deep RL method with the sawtooth potential (S9) with  $L = 1$  and  $U_0 = 5$ . The training results are shown in Fig. S2.

$$U(x) = \begin{cases} \frac{3U_0}{L}x & \text{for } 0 \leq x \leq \frac{L}{3} \\ U_0 - \frac{3U_0}{2L} \left(x - \frac{L}{3}\right) & \text{for } \frac{L}{3} < x < L, \end{cases} \quad \text{and } U(x+L) = U(x). \quad (\text{S9})$$

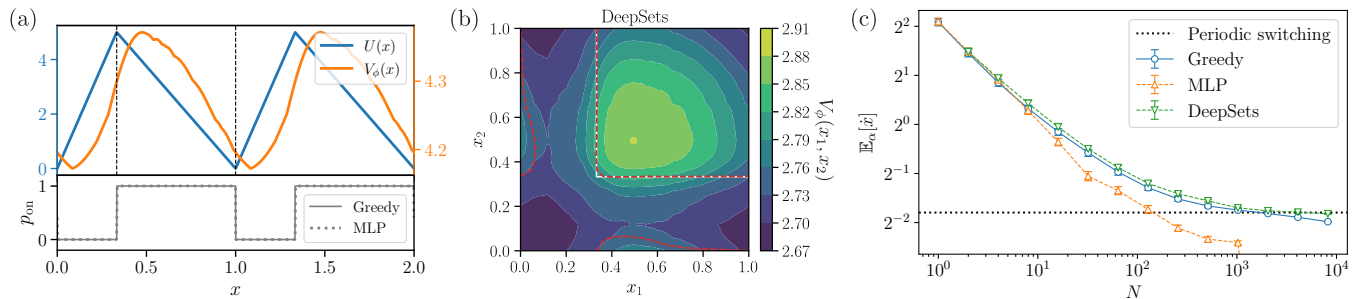


FIG. S2. Training results for the sawtooth potential. (a)  $N = 1$  case. Top: Sawtooth potential  $U$  (S9) and trained value network  $V_\phi$  as a function of position  $x$  are denoted by blue and orange lines, respectively. Bottom: The solid line denotes the probability of switching on the potential ( $p_{\text{on}}$ ) as a function of  $x$  for the greedy policy. The dotted line represents  $p_{\text{on}}$  of the trained MLP policy. (b)  $N = 2$  case. The decision boundaries of the trained DeepSets policy and the greedy policy are shown with the red dashed and solid white contours, respectively. (c) The current  $\mathbb{E}_\alpha[x]$  as function of  $N$  for each policy.

\* [hjeong@kaist.edu](mailto:hjeong@kaist.edu)

- [1] J. Schulman, F. Wolski, P. Dhariwal, A. Radford, and O. Klimov, Proximal policy optimization algorithms, [arXiv:1707.06347](https://arxiv.org/abs/1707.06347).
- [2] J. Achiam, Spinning Up in Deep Reinforcement Learning (2018), <https://spinningup.openai.com>.
- [3] J. Schulman, P. Moritz, S. Levine, M. Jordan, and P. Abbeel, High-Dimensional Continuous Control Using Generalized Advantage Estimation, in *International Conference on Learning Representations* (2016) [arXiv:1506.02438](https://arxiv.org/abs/1506.02438).
- [4] A. Paszke *et al.*, PyTorch: An Imperative Style, High-Performance Deep Learning Library, in *Advances in Neural Information Processing Systems 32* (Curran Associates, Inc., Vancouver, 2019) pp. 8024–8035.
- [5] D. P. Kingma and J. Ba, Adam: A Method for Stochastic Optimization, in *International Conference on Learning Representations* (2015) [arXiv:1412.6980](https://arxiv.org/abs/1412.6980).
- [6] V. Nair and G. E. Hinton, Rectified linear units improve restricted boltzmann machines, in *Proceedings of the 27th International Conference on Machine Learning* (Haifa, Israel, 2010) pp. 807–814.